

## Shear-Induced Layered Structure of Polymeric Micelles by SANS

Jun Jiang,<sup>\*,†</sup> Christian Burger,<sup>‡</sup> Chunhua Li,<sup>†</sup> Jun Li,<sup>§</sup> Min Y. Lin,<sup>⊥</sup> Ralph H. Colby,<sup>#</sup> Miriam H. Rafailovich,<sup>\*,†</sup> and Jonathan C. Sokolov<sup>†</sup>

Department of Materials Science and Engineering, State University of New York at Stony Brook, Stony Brook, New York 11794-2275; Department of Chemistry, State University of New York at Stony Brook, Stony Brook, New York 11794; Department of Physics, Queens College and Graduate Center, City University of New York, Flushing, New York 11367; Exxon Research and Engineering Corporation, Annadale, New Jersey 08801; and Department of Materials Science and Engineering, The Pennsylvania State University, University Park, Pennsylvania 16802

Received November 17, 2006; Revised Manuscript Received February 27, 2007

**ABSTRACT:** Small-angle neutron scattering (SANS), under shear using a Couette cell in radial and tangential scattering geometry, was performed to examine the structural evolution of the polymeric micellar macrolattice formed by concentrated aqueous solutions of triblock copolymer—poly(ethylene oxide)<sub>99</sub>—poly(propylene oxide)<sub>69</sub>—poly(ethylene oxide)<sub>99</sub> (Pluronic F127)—as a function of the shear rate. The micellar gel showed a shear thinning, i.e., a reduction of the resistance to shear, by forming a layered stacking of two-dimensional hexagonally close packed (HCP) polymer micelles. While traditional SANS experiments using a Couette shear cell are performed in radial geometry, we found the use of the tangential scattering geometry essential to obtain information on the layer stacking sequence. A theoretical model was developed to calculate 2D SANS scattering patterns that can be compared with the experimental data. We found that the micellar cores maintained their spherical shapes without deforming into ellipsoids and that the intralayer neighboring micelle center-to-center distance and the interlayer long period were independent of the shear rate and only depended on the concentration of the polymer. We also found that the stacking sequence changed from asymmetrically twinned ABC (i.e., FCC) at low shear rates to random AB stacking at high shear rates.

## Introduction

Because of their thermoreversible gelation property, concentrated solutions of nonionic amphiphilic triblock copolymers like poly(ethylene oxide)<sub>99</sub>—poly(propylene oxide)<sub>69</sub>—poly(ethylene oxide)<sub>99</sub> (PEO<sub>99</sub>—PPO<sub>69</sub>—PEO<sub>99</sub>, Pluronic F127) are being widely used in numerous biomedical applications, such as drug delivery and gels for replacing biological fluids.<sup>1,2</sup> While most traditional polymer gels are formed by a swollen network of covalently cross-linked polymer chains, the present triblock copolymer gel is held together by reversible entanglements between the coronae of neighboring micelles.<sup>3–6</sup> The reversible nature of the entanglements is due to the absence of covalent cross-linking between the micelles. The organization of micelles into layers adapted to laminar shear flow is responsible for the exceptional viscoelastic properties of these systems, especially when being subjected to shear forces. Consequently, the structure property relationships are dynamic and vary with the shear rate. Hence, it is important to understand their correlation with rheology as a function of the shear rate.

Since the pioneering work of Hoffman, Ackerson, and Loose<sup>7–9</sup> on shear-induced transitions in suspensions of charged particles, much effort has been made to identify the structural properties of colloidal crystals under shear. More recently,<sup>10,11</sup> it has been shown that the selective solvent properties of diblock or triblock copolyethers like poly(ethylene oxide) (PEO), poly(propylene oxide) (PPO), or poly(butylene oxide) (PBO) in

aqueous solution can lead to the formation of micelles with a spherical core–shell geometry (Figure 1a). While dilute solutions contain discrete micelles, concentrated solutions can form highly ordered arrangements of micelles, characterized by a certain overlap of the coronae of neighboring micelles (Figure 1b–d). Especially in a shear environment, the packing order is dominated by 2D hexagonally packed layers of micelles (Figure 1b), the vertical stacking of which approaches 3D close packings of spheres with the limiting cases of perfect ABC stacking sequence (Figures 1d and 2a), corresponding to a face-centered-cubic (FCC) structure, and perfect ABA stacking leading to the 3D hexagonally close-packed structure (Figure 2b), respectively, and their intermediates ranging from near ideal structures with moderate stacking faults to random stacking sequences (Figure 2c). As far as the structure under shear flow is concerned, a link has been established between the former conventional (charge-stabilized) colloidal crystals and the latter nonionic micellar close-packed phases. The ordering would drastically influence the flow properties of the dispersion because the layered structure would comply easily with the flow, thereby reducing the shear viscosity. This effect is known as “shear thinning”.

To build a 3D close packing of spheres, starting from a single 2D hexagonally packed layer of micelles (A) (Figure 1b) and adding a second layer (B) (Figure 1c), there are two possibilities for the addition of the next layer: either filling the “holes” visible in the projection (C) (Figures 1d and 2a), leading to an ABC stacking sequence, corresponding to a face-centered cubic (FCC) structure, or reverting back to the shift of the first layer (A), not depicted in Figure 1, leading to an ABA stacking sequence or 3D close-packed hexagonal structure (Figure 2b). The addition of further layers could proceed in an ordered fashion replicating an ABCABC or ABABAB stacking se-

\* Corresponding authors. E-mail: mrafailovich@notes.cc.sunysb.edu; jjiang@ic.sunysb.edu.

† Department of Materials Science and Engineering, SUNY, Stony Brook.

‡ Department of Chemistry, SUNY, Stony Brook.

§ City University of New York, Flushing.

⊥ Exxon Research and Engineering Corporation.

# The Pennsylvania State University.

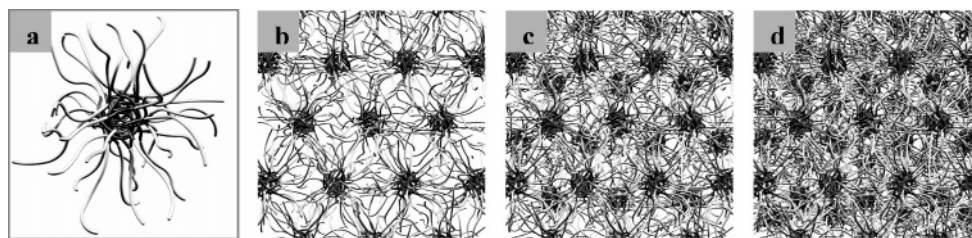


**Figure 1.** Schematic representations of Pluronic F127 micelles: (a) single micelle with spherical core-shell geometry; (b) single 2D hexagonally packed layer of micelles; (c) two 2D hexagonally packed layers of micelles (AB); and (d) three layers with ABC (or FCC) stacking sequence structure. (b–d) correspond to the radial geometry.

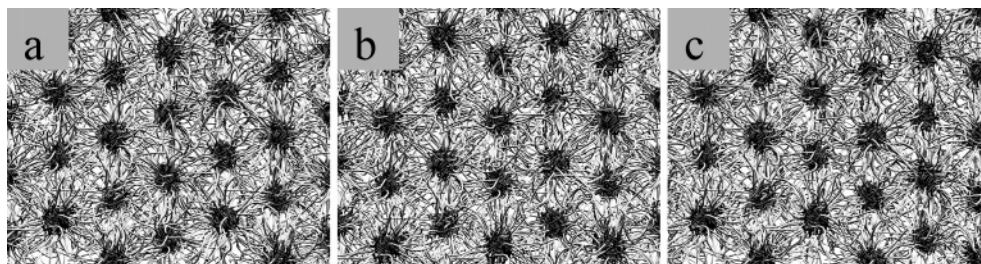


**Figure 2.** Tangential views of (a) ABC stacking sequence or FCC structure, (b) ABA stacking sequence or 3D hexagonal structure, and (c) random AB stacking sequence.

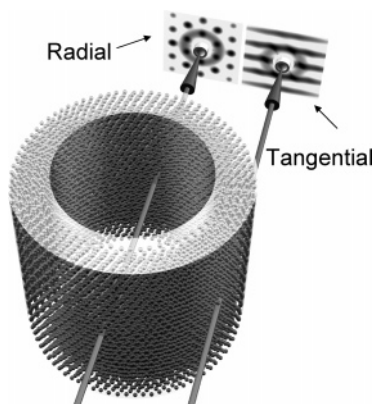


**Figure 3.** Configuration of the Couette cylinder used for the SANS measurements.

quence, or it could involve stacking faults (Figure 2c). From a comparison of Figure 1d and Figure 2a–c it is clear that the nature of the stacking order becomes much more obvious in Figure 2, viewed parallel to layer planes, rather than for Figure 1d, viewed perpendicular to the layer planes, where most information about the stacking sequence is lost in the projection.

It is crucial to understand that this situation directly translates to a scattering experiment in Couette shearing geometry (Figure 3). As expected, the layers of micelles are found to be arranged parallel to the cylinder surfaces of the outer and inner concentric Couette cylinders. Thus, the traditional Couette scattering geometry with the neutron beam centered at the Couette cell (“radial” geometry, Figure 3) corresponds to the perpendicular situation of Figure 1d, so that most information about the stacking sequence is lost in the projection onto the plane normal to the beam. In order to extract the stacking sequence information, an experiment in “tangential” geometry (Figure 3), corresponding to Figure 2, needs to be performed.

The system that we have investigated under shear is a “soft solid”, resulting from the aggregation of self-assembling triblock copolymers PEO<sub>99</sub>–PPO<sub>69</sub>–PEO<sub>99</sub> into spherical core-shell micelles (Figure 1a) and crystallizing into a 3D close-packed macrolattice.<sup>3,4</sup> The spherical micelle consists of a core of mainly the comparatively more hydrophobic PPO blocks (shown as dark in Figures 1 and 2) with a low water content, surrounded by a

water-swollen corona of PEO blocks (shown as light in Figures 1 and 2). At low polymer concentrations, light scattering measurements corroborate the aggregation of copolymers into spherical micelles and allow the determination of the micelle size. In the gel-like region the aggregation number (60–65) and also the micellar core radius size (4–5 nm) are not sensitive to concentration or temperature changes.<sup>3</sup>

The oriented structures of several similar copolymers under steady shear have been studied by SANS and SAXS.<sup>12–17</sup> For instance, using scattering techniques on both tangential and radial geometry, Molino, Diat, and Slawecski et al.<sup>12–15</sup> showed the shear orientation effects on the micelle system of Pluronic F85 and F108. In this work, we present several extensions to the theoretical scattering analysis by Loose and Ackerson<sup>8,9</sup> on which all previous data evaluation was based and apply it to experimental SANS data under shear for the F127 copolymer system.

### Experimental Section

Pluronic F127 (12 600 Da, 70% w/w PEO) was obtained from BASF (Mount Olive, NJ). Concentrations of Pluronic F127 solutions are expressed by weight percentage (% w/w). Pluronic was dissolved in deuterium oxide, obtained from Cambridge Isotope Laboratories, Inc., and kept stirring in an ice water mixture at 2 °C for 2 h. The solution was then refrigerated for 1–2 days until it cleared. Deuterium oxide was used to obtain good contrast and low background in the neutron scattering experiments.

The small-angle neutron scattering (SANS) experiments were performed at the National Institute of Standards and Technology (NIST) Reactor Division. Data were collected on an area-sensitive detector at the NG3 (NIST/Exxon/U.Minn) SANS beamline, with sample-to-detector distances of 3.45 m. The nominal wavelength of the neutrons was 0.60 nm with a dispersity  $\Delta\lambda/\lambda$  of 0.10 and an average incident intensity of  $\sim 464\,000$  neutrons/s, the accessible  $q$  range was from 0.055 to 0.969 nm<sup>-1</sup>, and the magnitude of the scattering vector is defined by  $q = (4\pi/\lambda) \sin(\theta/2)$ , where  $\theta$  is the angle between incident and scattered beams. The micellar solutions were placed inside a Couette apparatus designed for SANS experiments. This quartz Couette shearing setup consists of a fixed diameter rotor with several choices for the internal stator. The resulting scattering configuration for the steady shear experiments is outlined in Figure 3. The Couette cylinder could be shifted such that the incident beam could pass through the radial or the tangential

sample position, providing two different views of the structure corresponding to Figures 1 and 2, respectively. We chose a stator offering a 1 mm gap width. Samples were loaded carefully at 2 °C to minimize shear effects. Then the temperature was increased to 37 °C, where the sample was stabilized for 20 min before the onset of shear. The diffraction images represent the steady shear microstructure at the prescribed shear rate averaged over a 5–10 min integration time.

The steady shear stress vs shear rate data were collected from a strain-controlled rheometer, Rheometrics Fluids spectrometer II, using concentric cylinders with an inner diameter of 16.5 mm, an outer diameter of 17.1 mm, and 13.7 mm height. Temperature control was achieved using a water bath with concentric cylinders, and the temperature was determined from a thermocouple connected to the inner cylinder. Low-viscosity silicone oil was added on top of the surface of the sample to minimize evaporation of the solvent.

### Scattering Theory

The scattered intensity  $I$  of a system of stacked layers can be factorized into three components

$$I(\mathbf{q}) = F(\mathbf{q}) L(\mathbf{q}) Z(\mathbf{q}) \quad (1)$$

where  $F$  is the form factor of a single micelle,  $L$  is an intralayer lattice factor describing the arrangement of the micelles inside a single layer, and  $Z$  is an interlayer lattice factor describing the arrangement between the layers.

The scattering vector  $\mathbf{q}$  has the absolute value  $q = |\mathbf{q}| = 4\pi\lambda^{-1} \sin(\theta/2)$ , where  $\theta$  is the angle between incident and scattered beam and  $\lambda$  is the wavelength, and it has the components  $\mathbf{q} = (q_1, q_2, q_3)$  where  $q_1$  points tangentially in the Couette shear flow direction,  $q_2$  points into the direction of the Couette rotation axis, and  $q_3$  points radially perpendicular to the Couette shear flow direction (see Figure 3). Thus, in a Couette SANS experiment in *radial geometry*, we will measure a planar 2D section (neglecting Ewald sphere curvature effects) in the  $(q_1, q_2)$  plane with  $q_3 = 0$  through the total intensity distribution (1) in reciprocal space, and in *tangential geometry*, we will measure a section in the  $(q_3, q_2)$  plane with  $q_1 = 0$ .

Without significant loss of generality, we approximate the micelle form factor by its Guinier approximation

$$F(\mathbf{q}) = F(q) = \exp(-R_G^2 q^2/3) \quad (2)$$

where  $R_G$  is the radius of gyration, assuming that form factor minima and oscillations are averaged out due to polydispersity effects and due to the core-shell nature of the micelle and because the experimental  $q$  range is small enough. Equation 2 sufficiently describes our data, and for specific density profiles of the core and corona regions, the corresponding  $R_G$  could be calculated and compared with the one obtained from (2). Explicit expressions for the form factors of various core-shell morphologies are given in ref 18, but their use is not really warranted for the present data.

Inside a single layer of micelles, we assume a 2D hexagonal close-packed arrangement described by the real space unit cell vectors

$$\mathbf{a} = (1, \sqrt{3}, 0)a/2 \quad \text{and} \quad \mathbf{b} = (1, -\sqrt{3}, 0)a/2 \quad (3)$$

where  $a$  is the center-to-center distance between neighboring micelles, corresponding to a set of reciprocal space unit cell vectors

$$\mathbf{a}^* = (1, 1/\sqrt{3}, 0)2\pi/a \quad \text{and} \quad \mathbf{b}^* = (1, -1/\sqrt{3}, 0)2\pi/a \quad (4)$$

Note that there are two possible orientations for an aligned 2D hexagonal lattice: the unit hexagon standing on its edge or standing on its tip, and the on-edge orientation as depicted in Figure 1a and as defined by (3) and (4) for real and reciprocal space corresponds to the experimentally observed one, as follows from the agreement of the orientation of experimental and calculated radial patterns (see Figures 5 and 6).

For the 2D hexagonal arrangement defined by these unit cell vectors, the intralayer lattice factor  $L$  is given by

$$L(\mathbf{q}) = \sum_{h=-\infty}^{\infty} \sum_{k=-\infty}^{\infty} w_{hk}^{-2} \exp(-\pi w_{hk}^{-2} |\mathbf{q} - h\mathbf{a}^* - k\mathbf{b}^*|^2) \quad (5)$$

where we have assumed the individual peak shapes to be given by Gaussians of integral widths  $w_{hk}$  which may depend on the Miller indices  $h$  and  $k$ . It would be straightforward to use different peak shapes, but Gaussians appear to work well for our experimental data.

In order to speed up the calculation, we replace the exact expression (5) by the approximation

$$\tilde{L}(\mathbf{q}) = w_{hk}^{-2} \exp\left(-\frac{\pi^2}{a^2 w_{hk}^2} \left\{ \sin^2\left[\frac{aq_1}{2}\right] + \sin^2\left[\frac{a}{4}(q_1 + \sqrt{3}q_2)\right] + \sin^2\left[\frac{a}{4}(q_1 - \sqrt{3}q_2)\right] \right\}\right) \quad (6)$$

which is good for sufficiently narrow and well-separated peaks and calculates much faster than the original (5).

Assuming the average distance from one layer to the next is that of an ideal close packing of spheres, so that neighboring micelles between layers also have a center-to-center distance  $a$ , there are two possible translation vectors

$$\mathbf{t}_1 = (0, 1/\sqrt{3}, \sqrt{2/3})a \quad \text{and} \quad \mathbf{t}_2 = (0, -1/\sqrt{3}, \sqrt{2/3})a \quad (7)$$

which describe the relative positioning from one layer to the next. If the interlayer distance deviates from the ideal value, (7) can be adjusted accordingly. Translational disorder can be introduced by displacing the translation vectors  $\mathbf{t}_{1,2}$  by vectors  $(\Delta_1, \Delta_2, \Delta_3)$  where the displacement components  $\Delta_{1,2,3}$  can be different for different directions of space and are taken to be normally distributed with standard deviations  $\sigma_{1,2,3}$ . This adjustable translational disorder can be used to analytically describe the effects of layer sliding or, after a straightforward modification of (9), for a “zigzag path” movement of the layers. Note that this constitutes a significant step beyond the treatment of Loose and Ackerson,<sup>9</sup> who consider discrete translational displacements only. Curiously, Molino et al.<sup>14</sup> using the Ackerson–Loose treatment describe the generalization to a continuum of displacements as a “formidable task” while the present work shows that it is, in fact, a minor modification, e.g., by extending the well-known chain of independent events model by Hermans<sup>19</sup> to the following dependent statistics.

In order to take stacking sequence correlations in first order into account, we assume that the layer stacking sequence can be described by a first-order Markov process. Its lattice factor can be summed in close form using matrix techniques.<sup>20</sup> Let the probability that a translation  $\mathbf{t}_j$  be followed by a translation  $\mathbf{t}_k$  be given by  $p_{jk}$ , where  $j$  and  $k$  can assume the values 1 or 2. Since  $p_{j1} + p_{j2} = 1$ , there are only two independent probabilities, say  $p_{11}$  and  $p_{22}$ . The probability  $p_j$  of finding a translation vector  $\mathbf{t}_j$  can be obtained from  $p_j = p_1 p_{1j} + p_2 p_{2j}$  and  $p_1 + p_2 = 1$ . Under these conditions, the interlayer lattice factor  $Z = Z(\mathbf{q})$  is given by

$$Z = 1 + 2\text{Re}\left\{\begin{pmatrix} p_1 & H_1 \\ p_2 & H_2 \end{pmatrix}^T \begin{bmatrix} 1 & 0 \\ 0 & 1 \end{bmatrix} - \begin{pmatrix} p_{11}H_1 & p_{12}H_2 \\ p_{21}H_1 & p_{22}H_2 \end{pmatrix}^{-1} \begin{pmatrix} 1 \\ 1 \end{pmatrix}\right\} \quad (8)$$

where

$$H_j(\mathbf{q}) = \exp[i\mathbf{q}\mathbf{t}_j - (\sigma_1^2 q_1^2 + \sigma_2^2 q_2^2 + \sigma_3^2 q_3^2)/2] \quad (9)$$

is the Fourier transform of the distribution of translations of the  $j$  type including their disordering displacements.

Note that (8) differs from eq A2 in Loose and Ackerson<sup>9</sup> where those authors incorrectly assume  $p_1 = p_2 = 1/2$  to be valid in the general case. Setting  $p_1 = p_2$  implies  $p_{11} = p_{22}$ , a specialization Loose and Ackerson eventually introduced in their eq A7 so that their final result is correct again within this limitation, but the exact general solution (8) or (10), even including the generalization to continuous sliding, is not much more complicated than Loose and Ackerson's expressions. The specialization  $p_{11} = p_{22}$  assumes that all regions with predominantly ABC stacking sequences are accompanied by equal amounts of ACB regions (twinning) and appears unmotivated in the present anisotropic shear environment; it is, in fact, not compatible with some of our data obtained in tangential Couette geometry (see, e.g., the first pattern in Figure 7) which is much more sensitive to these effects than the traditional radial geometry.

Equation 8 can be rewritten in the following form which is directly suitable for the calculation:

$$Z = \text{Re}\{2 - p_{11} - p_{22} + [2 - (p_{11} + p_{22})(2 - p_{11})]H_1 + [2 - (p_{11} + p_{22})(2 - p_{22})]H_2 + (1 - p_{11} - p_{22})(2 - p_{11} - p_{22})H_1H_2\} \{ (2 - p_{11} - p_{22})[1 - p_{11}H_1 - p_{22}H_2 - (1 - p_{11} - p_{22})H_1H_2] \}^{-1} \quad (10)$$

## Results and Discussion

Figure 4 shows the steady shear viscosity as a function of the shear rate for the micellar gel of 20% F127 in water. From the figure we can see that the viscosity decreased with increasing shear rate; i.e., the gel is a shear thinning system. The insert of oscillatory frequency sweep shows that this material is in fact a solid. This result had been previously reported by Prud'homme et al., who described the shear rate dependence of the viscosity of such non-Newtonian fluids by using a Carreau-like model,  $\eta = \eta_0/(1 + (a\dot{\gamma})^b)$ , where  $a$  and  $b$  are two coefficients related to volume fraction and properties of the micelles.<sup>21</sup> This decrease of the viscosity indicates that the 2D hexagonally close-packed layers of micelles form shear planes which are arranged to minimize the resistance against laminar flow.

Figure 5a–i shows the experimental scattering patterns of 20% F127 in D<sub>2</sub>O, obtained in the radial scattering geometry, with increasing shear rate from 0 to 600 1/s. The corresponding tangential scattering patterns are shown in Figure 7a–i.

The model discussed in the theoretical section allows the calculation of 2D SANS scattering patterns that can be compared to the experimental data. Figures 6 and 8 show calculated patterns for radial and tangential scattering geometry, respectively, with parameters semiquantitatively adjusted by trial and error to produce the best visual agreement with the experimental patterns. Many of the structural parameters of interest are quite sensitive to small changes and can be obtained with good accuracy from these comparisons (e.g., micelle center-to-center distance  $a$  error <1%, micelle core radius  $R$  error <5%). The stacking sequence probabilities  $p_{11}$  and  $p_{22}$  are less sensitive,

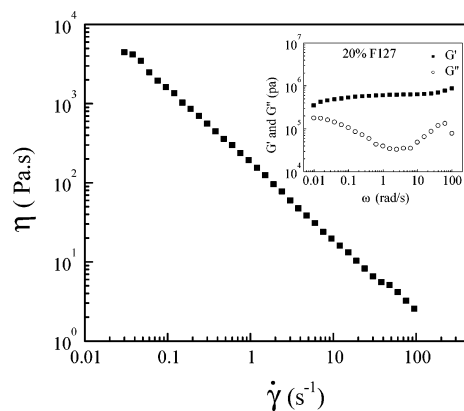


**Figure 4.** Steady shear viscosity  $\eta$ , as a function of the shear rate  $\dot{\gamma}$ , on a micelle gel of 20% Pluronic F127 in D<sub>2</sub>O.

especially in radial scattering geometry (for the tangential patterns we would estimate an error around <20%).

Furthermore, it was found to be necessary to include an isotropic component in form of one or two scattering rings in the calculated patterns. As a function of the shear rate, the volume fraction of the isotropic component decreased from about 0.999 for zero shear to about 0.7 for a shear rate of 600 1/s, indicating a continuing transformation of unoriented domains into the shear-aligned orientation.

The stacking sequence probabilities were found to change from  $p_{11} = 0.9$  and  $p_{22} = 0.7$  (Figure 8a) for a zero shear rate down to  $p_{11} = 0.5$  and  $p_{22} = 0.5$  (Figure 8i) for the shear rate of 600 1/s. This change of the stacking sequence probabilities suggests a structure change from asymmetrically twinned ABC (FCC) at low shear rates to a random AB stacking sequence at high shear rates. The clear texture (Figure 7a) observed in samples exposed to zero shear could be due to surface-induced micelle crystallization at the cylinder surface during the gelation process when increasing the temperature from 2 to 37 °C.<sup>22</sup> Note again that most of this information cannot be obtained in radial scattering geometry.

The intralayer neighboring micelle center-to-center distance  $a$  depends on the concentration of the polymer. By analyzing the experimental scattering patterns, we found that the distances between intralayer neighboring micelle are 20.5 and 19.2 nm for 20% and 30% polymer solutions, respectively. From these numbers, we can see that the micelle distance gets smaller due to the closer packing of micelles by increasing the polymer concentration. This distance did not change as a function of the shear rate.

The interlayer neighboring micelle center-to-center distance  $|\mathbf{t}_1| = |\mathbf{t}_2|$  only influences the tangential patterns and has no effect on the radial patterns. From the experimental tangential patterns, we found no need to adjust this parameter from its ideal value  $a$  for a 3D close packing of spheres.

The stacking sequence translational shift parameters  $\sigma_1$ ,  $\sigma_2$ , and  $\sigma_3$  were all taken to be 1 nm for most calculated patterns, indicating a moderate amount of translational disorder both parallel and perpendicular to the shearing planes.

The micellar core radius of gyration  $R_g$  (assuming an idealized core-shell scattering length density profile; for a more realistic nonconstant corona density profile, this is to be understood as some sort of apparent or equivalent radius) was found as  $R_g = 6.5$  nm, independent of the shear rate.

It is conceivable that under shear the micellar cores could deform from an ideal spherical to an ellipsoidal shape. This effect could be taken into account by subjecting the micellar form factor to the reciprocal deformation. Within the accuracy

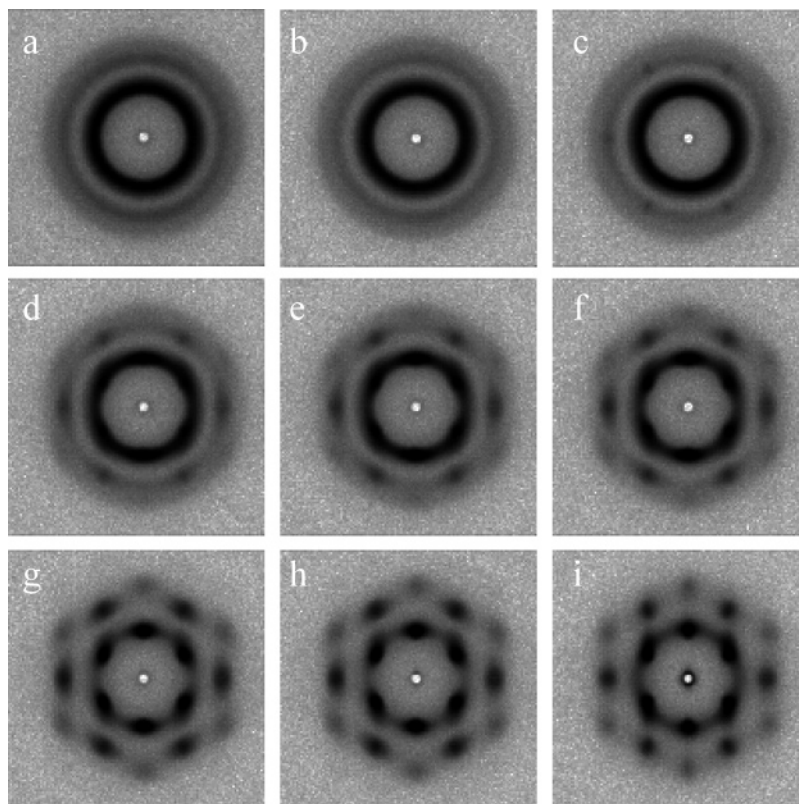


**Figure 5.** SANS radial scattering patterns from a to i for a 20% Pluronic F127 gel as a function of the shear rate: 0, 0.01, 1, 5, 10, 15, 30, 50, and 600 1/s.

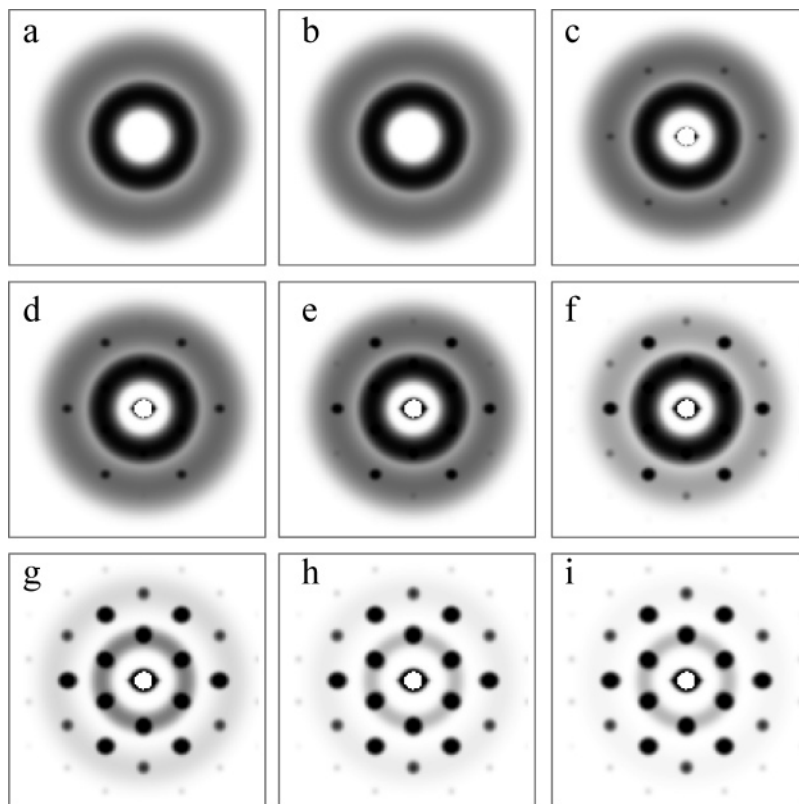


**Figure 6.** Calculated radial scattering patterns from a to i for a 20% Pluronic F127 gel, adapted for the experimental SANS patterns of Figure 5.

of our experiments and analysis, an undeformed micelle form factor was found to sufficiently describe the experimental data. Thus, we did not observe this type of deformation. The layered structure was stable even up to shear rates of 1000 1/s.

#### Conclusion

Small-angle neutron scattering (SANS) experiments in radial and especially tangential scattering configurations were performed to examine the shear rate dependence of the micellar

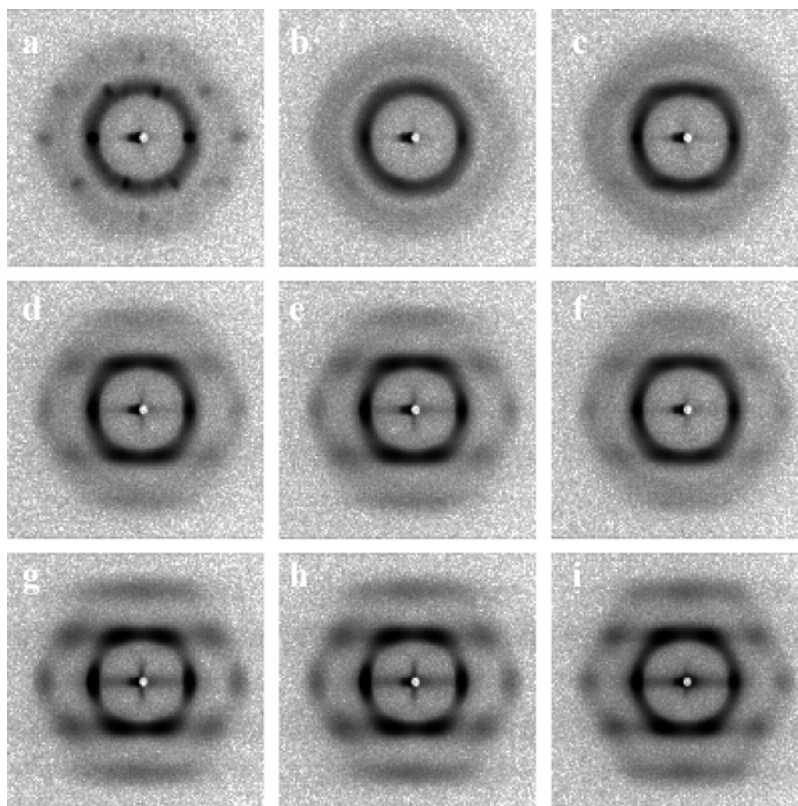


**Figure 7.** SANS tangential scattering patterns from a to i for a 20% Pluronic F127 gel as a function of the shear rate: 0, 0.01, 1, 5, 10, 15, 30, 50, and 600 1/s.

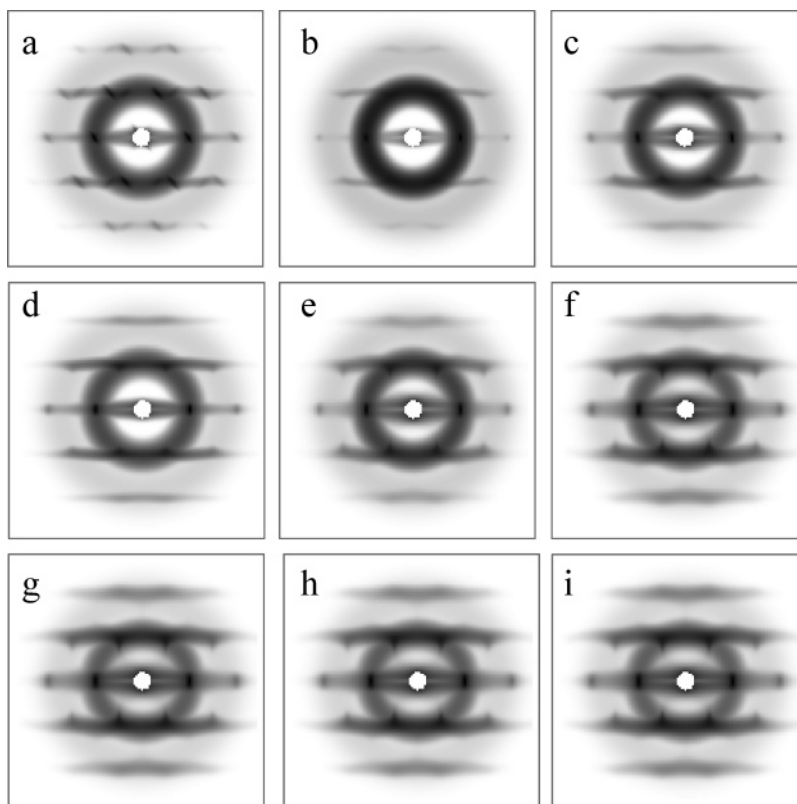


**Figure 8.** Calculated tangential scattering patterns from a to i for a 20% Pluronic F127 gel, adapted for the experimental SANS patterns of Figure 7.

macrolattice formed by concentrated aqueous solutions of triblock copolymer—poly(ethylene oxide)<sub>99</sub>—poly(propylene oxide)<sub>69</sub>—poly(ethylene oxide)<sub>99</sub> (Pluronic F127)—subjected to in-situ steady shear. The micellar gel showed a shear thinning

behavior to reduce the resistance to shear by forming a layered stacking of two-dimensional HCP micelles. An experiment in “tangential” scattering provided us the most stacking sequence information. A theoretical model was developed to calculate

the scattering intensity distribution in 3D reciprocal space for oriented stacks of micellar layers with stacking sequences following a first-order Markov process, allowing for disorder effects and having ideal cubic and hexagonal close packings as its limiting cases. 2D sections through these calculated 3D intensity distributions were compared to experimental SANS scattering patterns. The model developed could be applied to other systems, such as layered packings of ionic copolymer micelles or other particles, and also to nonparticulate layered systems like graphite or clay. The ability to understand the essential relationships between hydrogel structure and its rheological response could have numerous applications for hydrogel implants under physiological conditions.

**Acknowledgment.** Support of this work by the NSF-MRSEC is gratefully acknowledged.

### References and Notes

- (1) Chun, K. W.; Lee, J. B.; Kim, S. H.; Park, T. G. *Biomaterials* **2005**, *26*, 3319–3326.
- (2) Cohn, D.; Sosnik, A.; Garty, S. *Biomacromolecules* **2005**, *6*, 1168–1175.
- (3) Wu, C.; Liu, T.; Chu, B.; Schneider, D. K.; Graziano, V. *Macromolecules* **1997**, *30*, 4574–4583.
- (4) Mortensen, K.; Talmon, Y. *Macromolecules* **1995**, *28*, 8829–8834.
- (5) Wanka, G.; Hoffmann, H.; Ulbricht, W. *Macromolecules* **1994**, *27*, 4145–4159.
- (6) Mortensen, K. *J. Phys.: Condens. Matter* **1996**, *8*, A103–A124.
- (7) Hoffman, R. L. *Trans. Soc. Rheol.* **1972**, *16*, 155–173.
- (8) Ackerson, B. J.; Clark, N. A. *Phys. Rev. Lett.* **1981**, *46*, 123–126.
- (9) Loose, W.; Ackerson, B. J. *J. Chem. Phys.* **1994**, *101*, 7211–7220.
- (10) Castelletto, V.; Hamley, I. W.; Holmqvist, P.; Rekasas, C.; Booth, C.; Grossmann, J. G. *Colloid Polym. Sci.* **2001**, *279*, 621–628.
- (11) Daniel, C.; Hamley, I. W.; Mingvanish, W.; Booth, C. *Macromolecules* **2000**, *33*, 2163–2170.
- (12) Diat, O.; Porte, G.; Berret, J.-F. *Phys. Rev. B* **1996**, *5*, 14869–14872.
- (13) Berret, J.-F.; Molino, F. R.; Porte, G.; Diat, O.; Lindner, P. *J. Phys.: Condens. Matter* **1996**, *8*, 9513–9517.
- (14) Molino, F. R.; Berret, J.-F.; Porte, G.; Diat, O.; Lindner, P. *Eur. Phys. J. B* **1998**, *3*, 59–72.
- (15) Slawecki, T. M.; Glinka, C. J.; Hammouda, B. *Phys. Rev. E* **1998**, *58*, R4084–R4087.
- (16) McConnell, G. A.; Lin, M. Y.; Gast, A. P. *Macromolecules* **1995**, *28*, 6754–6764.
- (17) Hamley, I. W. *J. Phys.: Condens. Matter* **2001**, *13*, 643–671.
- (18) Förster, S.; Burger, C. *Macromolecules* **1998**, *31*, 879–891.
- (19) Hermans, J. J. *Rec. Trav. Chim. Pay-Bas* **1944**, *63*, 211–218.
- (20) Hendricks, S.; Teller, E. *J. Chem. Phys.* **1942**, *10*, 147–167.
- (21) Prud'homme, R. K.; Wu, G.; Schneider, D. K. *Langmuir* **1996**, *12*, 4651–4659.
- (22) Wu, C.; Liu, T.; White, H.; Chu, B. *Langmuir* **2000**, *16*, 656–661.

MA062654J